frontiers | Frontiers in Earth Science

TYPE Original Research
PUBLISHED 15 January 2025
DOI 10.3389/feart.2024.1481614

OPEN ACCESS

EDITED BY
Luigi Jovane,
University of São Paulo, Brazil

REVIEWED BY
Jing Bi,
Guizhou University, China
Zhanping Song,
Xi'an University of Architecture and Technology, China

*CORRESPONDENCE
Hong Zhang,
✉ 810630109@qq.com

RECEIVED 16 August 2024
ACCEPTED 20 December 2024
PUBLISHED 15 January 2025

CITATION
Zhang H, Gao R, Luo H, Chen P and Liu H (2025) Study on the side friction resistance capacity of prefabricated pipe piles in coral reef strata.
Front. Earth Sci. 12:1481614.
doi: 10.3389/feart.2024.1481614

Study on the side friction resistance capacity of prefabricated pipe piles in coral reef strata

Hong Zhang[1]*, Ran Gao[1,2], Huiwu Luo[1], Peishuai Chen[1] and Haifeng Liu[3]

[1]CCCC Second Harbour Engineering Company Ltd., Wuhan, Hubei, China, [2]College of Civil Engineering, Chongqing University, Chongqing, China, [3]State Key Laboratory of Geomechanics and Geotechnical Engineering, Institute of Rock and Soil Mechanics, Chinese Academy of Sciences, Wuhan, China

Coral reefs are widely distributed along the "Maritime Silk Road", and their unique mechanical properties pose numerous challenges for marine engineering construction. The side friction resistance (SFR) capacity of traditional driven piles in coral reef strata remains unclear, and there is a lack of effective calculation methods. Furthermore, the complex marine environment imposes higher requirements on pile foundation construction and durability. In this study, a series of interfacial shear tests were carried out for coral sand and coral reef limestone (CRL) in the sea area near the Maldives islands and reefs, and the distribution law of the SFR of prefabricated pipe piles in coral sand was investigated by using a large-scale pile foundation model test apparatus. The interfacial shear behavior of the coral sand is similar to that of the crushed coral reef limestone, both of which experience ideal elastic-plastic changes, with an interfacial friction angle of approximately 35°. The ultimate SFR of the prefabricated pipe piles in coral sand increases gradually and then plateaus, and the distribution of the SFR along the depth direction can be simplified as a combination of triangular and rectangular patterns. Based on the distribution law of the pile SFR, this study establishes a modified formula for calculating SFR of the pile in coral sand, which is verified by comparing the calculated SFR capacity of driven piles of the China-Maldives Friendship Bridge with the results of the field test piles. This study provides an important theoretical basis and practical guidance for the design and construction of pile foundation engineering in coral reef sea areas such as Maldives.

KEYWORDS

coral reef geology, interfacial shear, model tests, side friction resistance capacity, side friction resistance formula

1 Introduction

A large number of coral reefs are distributed in the offshore areas along the "Maritime Silk Road", and there is a great potential for the development of bridge engineering connecting the islands. Coral reefs, as a unique geological structure in tropical and subtropical regions, have special engineering mechanical properties due to their unique formation mechanism and geological characteristics (Kong and Fonseca, 2018; Zhou et al., 2022; Gao and Ye, 2023;

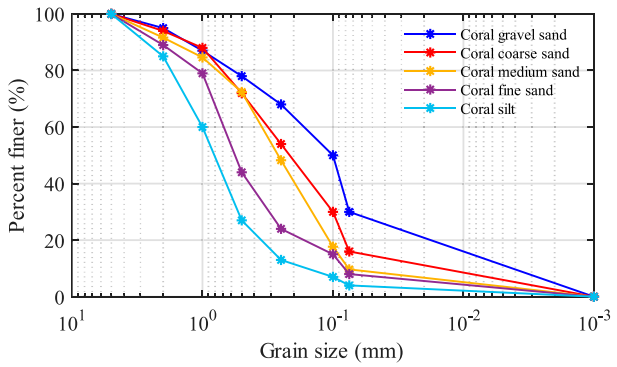

FIGURE 1
The GSD curves of coral sand particles used in this study.

Yao et al., 2024), which bring many challenges and obstacles for engineering construction. With the unprecedented surge in tourism and intensified resource exploitation activities, marine engineering has flourished significantly, facilitating the construction of offshore facilities and the exploration of underwater resources (Chortis et al., 2020; Lin et al., 2019). Pile, as a conventional foundation form, is widely used in engineering construction due to its ability to traverse soft or liquefied soil layers. It can effectively transfer loads from the structure's base to deeper, more stable solid soil layers or bedrock. This load transfer is achieved either by end-bearing on the stable layer or by side friction against the soil along the pile shaft. And it has good compressive and pulling resistance, and can reduce the settlement of the structure. (Guo et al., 2018; Li and Deng, 2018; Höppner and Boley, 2022; Ho et al., 2022; Malik et al., 2016; Xu et al., 2023; Schmüdderich et al., 2020). Most of the existing studies focuses primarily on pile-soil interactions in conventional foundations (Achmus et al., 2009; Guo, 2006; Karthigeyan et al., 2006; Zhao et al., 2021; Bi et al., 2015), the effect of seawater corrosion and wave current on pile foundation is rarely considered (Song et al., 2018; Fan et al., 2023). whereas experimental data on coral sands remains limited (Ding et al., 2023; Dyson and Randolph, 2001; Peng et al., 2023; Wang et al., 2022; Wang et al., 2021b). This limitation necessitates the conduct of further corresponding research. In coral reef strata, pile foundation construction necessitates a thorough consideration of geological characteristics that differ significantly from those on land, including high porosity, low density, and high compressibility. The study of the bearing characteristics of pile foundations in coral reef strata is of paramount importance in ensuring project safety and enhancing construction efficiency (Fahey and Jewell, 1988; Ghazali et al., 1988).

The biggest engineering problem of coral reef sand due to its unique mechanical properties is the low SFR at the pile-soil interface. Angemeer et al. (1975) conducted pile loading tests in the North West Gulf of Australia, and the results indicated that the residual SFR of driven piles ranged from 13 to 18 kPa. They thus recognized the unusual properties of the coral sand and the apparent differences in pile loading tests and driven pile tests, and concluded that the traditional pile bearing capacity analysis method was not suitable for coral sand materials. Poulos and Randolph (1988) derived that the SFR of the coral sand in the test region was as low as 10–40 kPa through a series of conduit loading tests at the North Rankin offshore gas platform in western Australia. Agarwal et al. (1977), Dutt and Cheng (1984) also concluded that the SFR of steel pipe piles in coral reef geology was remarkably low through *in-situ* tests. The analysis of the pull-out test revealed that during the dynamic pile driving process, the cement within the coral sand particles surrounding the pile was partially destroyed, and the residual cement formed an arch-like structure, which led to a reduction in the horizontal stress on the pile side. Jiang et al. (2018) also observed that the decrease in horizontal effective stress on the pile side caused by particle crushing was significantly greater than the increase in horizontal effective stress resulting from compacting action. Meanwhile, the presence of numerous small cave-like holes induced by the soluble nature of carbonates and the unique natural deposition pattern of coral reef sands also contribute to the low SFR of the pile foundation (Zhou, 2014).

Wang et al. (2019) conducted various modified direct shear tests on the interface between calcareous sand and steel with different roughness, and noted that under the same interface test condition, the interfacial friction angle of calcareous sand and steel was generally 5°–6° larger than that observed for quartz sand. Zhu et al. (2015) investigated the characteristics of the static lateral pressure coefficient K_0 of coral sand and siliceous sand considering the water content through consolidation tests. They found that the K_0 of coral sand was less than that of siliceous sand at a low water content and was similar to siliceous sand at a high water content, and that changes in water content had a limited effect on the K_0 of calcareous sand. Xu et al. (2022) studied the shear mechanical properties of the pile-coral sand interface at different temperatures, confining pressures, and salinities for coral sands taken from the South China Sea. It is revealed that temperature had no significant impact on the surface characteristics of the pile and coral sand, and that the saline environment would weaken the shear strength of the interface to some extent. Qin et al. (2019) reported that the bearing state of the

TABLE 1 Basic physical parameters of coral sand for the test.

Parameters	Coral gravel sand	Coral coarse sand	Coral medium sand	Coral fine sand	Coral silty
d_{50}	1.00	0.58	0.26	0.22	0.15
Uniformity coefficient C_u	16.67	8.70	4.88	4.00	2.67
Curvature coefficient C_c	1.50	1.07	0.91	0.87	0.54
Grading	Well-graded	Well-graded	Poorly graded	Poorly graded	Poorly graded

TABLE 2 Basic physical parameters of crushed CRL.

Parameters	Crushing load 250 kN	Crushing load 500 kN	Crushing load 1,000 kN	Crushing load 1,500 kN	Crushing load 2000 kN
d_{50}	8.77	6.25	1.92	2.66	2.03
Uniformity coefficient C_u	47.06	48.49	37.64	36.60	33.93
Curvature coefficient C_c	4.52	2.11	0.49	0.69	0.69
Grading	Poorly graded	Poorly graded	Poorly graded	Poorly graded	Poorly graded

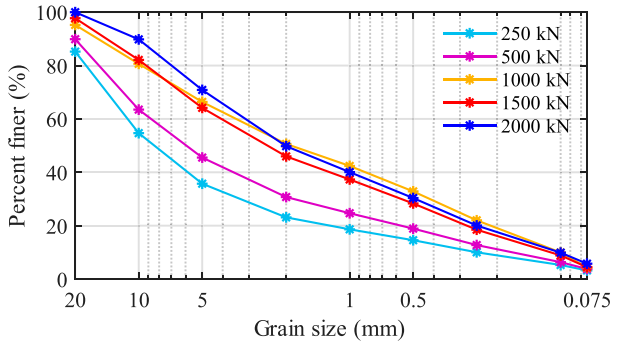

FIGURE 2
The GSD curves of crushed CRL used in this study.

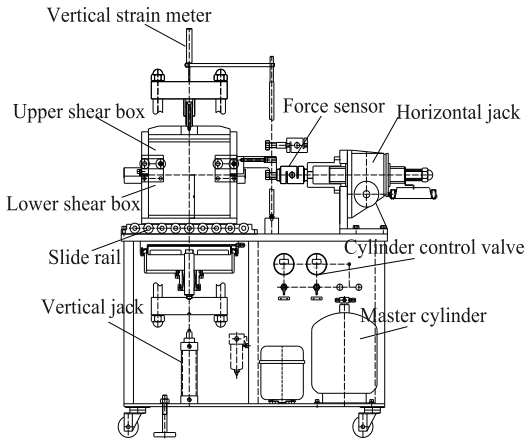

FIGURE 3
Self-developed large-scale specialized direct shear apparatus.

pile was significantly correlated with the depth of pile penetration, and the peak value of pile tip resistance occurred when the depth of pile penetration was more than 15 times the diameter of the pile. The depth of penetration and the magnitude of penetration energy affect the fragmentation degree of coral particles, which significantly affects the bearing capacity of pile in coral reef strata. Liu HF. et al. (2021) carried out the constant normal stiffness direct shear test on the interface between the pile and the coral reef calcarenite sample. It is shown that the shear strength of the pile-rock interface increases as the applied normal stress increases. The dilation of the shear failure surface after the peak strength decreases as the applied normal stress increases.

There have been related studies revealing the mechanism of low SFR at the pile-soil interface of driven piles in coral sand. However, there are no theoretical large-scale model tests for verification, nor are there established SFR distribution forms or suggested values for standard ultimate SFR. In view of this, the objective of this study is to thoroughly explore the SFR capacity of prefabricated pipe piles in coral reef strata. Herein, interfacial shear tests and model tests involving prefabricated pipe piles in calcareous sand are conducted based on the pile foundations of the China-Maldives Friendship Bridge project. The ultra-weak fiber Bragg grating (UWFBG) technique is adopted to monitor the deformation and internal force of the model piles, and the vertical effective stress grading loading technique is utilized to simulate the actual working conditions of driven piles at varying depths. The distribution law of pile SFR in coral sand with the increase of vertical effective stress around the pile at varying depths is investigated, while the function mechanism of pile SFR is analyzed, and a modified method for calculating the SFR of pile foundation in coral reef sand is proposed. This study contributes to strengthen the understanding of the bearing characteristics of pile foundations in coral reef strata and provides a robust guarantee for the safety and economy of related projects.

2 Experimental program

2.1 Material

The coral sand and coral reef limestone samples used in this study were taken from the sea area near the Maldives islands and reefs for the China-Maldives Friendship Bridge project. The coral sand samples are grayish-white loose sand without cementation, whose main components are calcium carbonate and a small amount of magnesium carbonate and other compounds. The surface of the particles is very rough, with a large number of microscopic internal cavities structures, and the shape of the

TABLE 3 Interfacial shear test conditions.

Test No.	Normal stress (kPa)	Dry density (g/cm^3)	Shear rate (mm/min)
S-1	25, 50, 100, 200, 400, 800	1.45	1.0
S-2	25, 50, 100, 200, 400, 800		
S-3	25, 50, 100, 200, 400, 800		
S-4	25, 50, 100, 200, 400, 800		
S-5	25, 50, 100, 200, 400, 800		
C-1	50, 100, 200, 400	1.45	1.0
C-2	50, 100, 200, 400		
C-3	50, 100, 200, 400		
C-4	50, 100, 200, 400		
C-5	50, 100, 200, 400		

Note: S1-S5 represent the coral gravel sand, coral coarse sand, coral medium sand, coral fine sand, and coral silty, respectively. C1-C5 represent crushed coral reef limestone under loads of 250 kN, 500 kN, 1,000 kN, 1,500 kN, and 2,000 kN, respectively.

particles is irregular. After the particle sieving test, the sampled coral sand can be divided into five categories according to the specification, i.e., coral gravel sand, coral coarse sand, coral medium sand, coral fine sand, and coral silty. The corresponding grain size distribution (GSD) curves are displayed in Figure 1. The basic physical parameters of coral sand at each grading are listed in Table 1.

In the process of pile foundation penetrating the coral reef limestone strata, the huge stress concentration at the pile tip can result in the crushing of the surrounding coral reef limestone. To simulate the shearing behavior of the pile foundation within the crushed coral reef limestone strata, the universal testing machine is utilized to crush the coral reef limestone samples and subsequently conduct shearing tests. Five different crushing load conditions, 250 kN, 500 kN, 1,000 kN, 1,500 kN, and 2000kN, are set respectively to obtain the rock crushing and particle grading of coral reef limestone under different crushing load conditions, and the GSD curves are presented in Figure 2, The basic physical parameters are listed in Table 2.

2.2 Test plan and test instruments

This study aims to investigate the SFR capacity of prefabricated pipe piles in coral reef strata, and to carry out the shear tests at the interfaces between coral sand, crushed coral reef limestone and concrete. Due to the large size and inhomogeneity of sample particles, this study has developed a large-scale specialized direct shear apparatus (as shown in Figure 3), with a 15 cm cubic shear box, a sensor capacity ranging from 0 to 50 kN, and a testing accuracy of 0.01 kN. The direct shear apparatus integrates the common features of direct shear and consolidation, realizing "one machine, multi-function". It is capable of conducting tests on the mechanical properties of the interface between structure and geotechnical soil, the soil strength, and the analysis of residual strength, etc. Furthermore, its pre-pressure and auxiliary cylinders are meticulously designed to precisely control the sample compactness and to solve the problem of large dispersion of test samples.

In this study, five types of coral sand-concrete interfacial shear tests and crushed coral reef limestone-concrete interfacial shear tests are conducted to analyze the interfacial shear curves and the variation of strength with normal stress, and to reveal the SFR capacity of prefabricated pipe piles in coral reef strata. The density of the sample is set at 1.45 g/cm^3, with dimensions of 150 mm × 150 mm × 150 mm. During the test, the interface is maintained in a saturated state. The test is configured with six normal stress conditions: 25 kPa, 50 kPa, 100 kPa, 200 kPa, 400 kPa, and 800 kPa, with a shear rate of 1.0 mm/min, and the specific test conditions are presented in Table 3.

3 Interfacial shear test

3.1 Results from coral sand - concrete interfacial shear test

The results of 5 types of coral sand-concrete interfacial shear tests are presented in Figure 4, and the variations in the interfacial shear strength among the 5 types of coral sand-concrete materials are basically consistent. As the shear strain increases, the interfacial shear stress experiences a gradual increase to a stable level, after a long stable stage, the strength may increase or decrease slightly. The

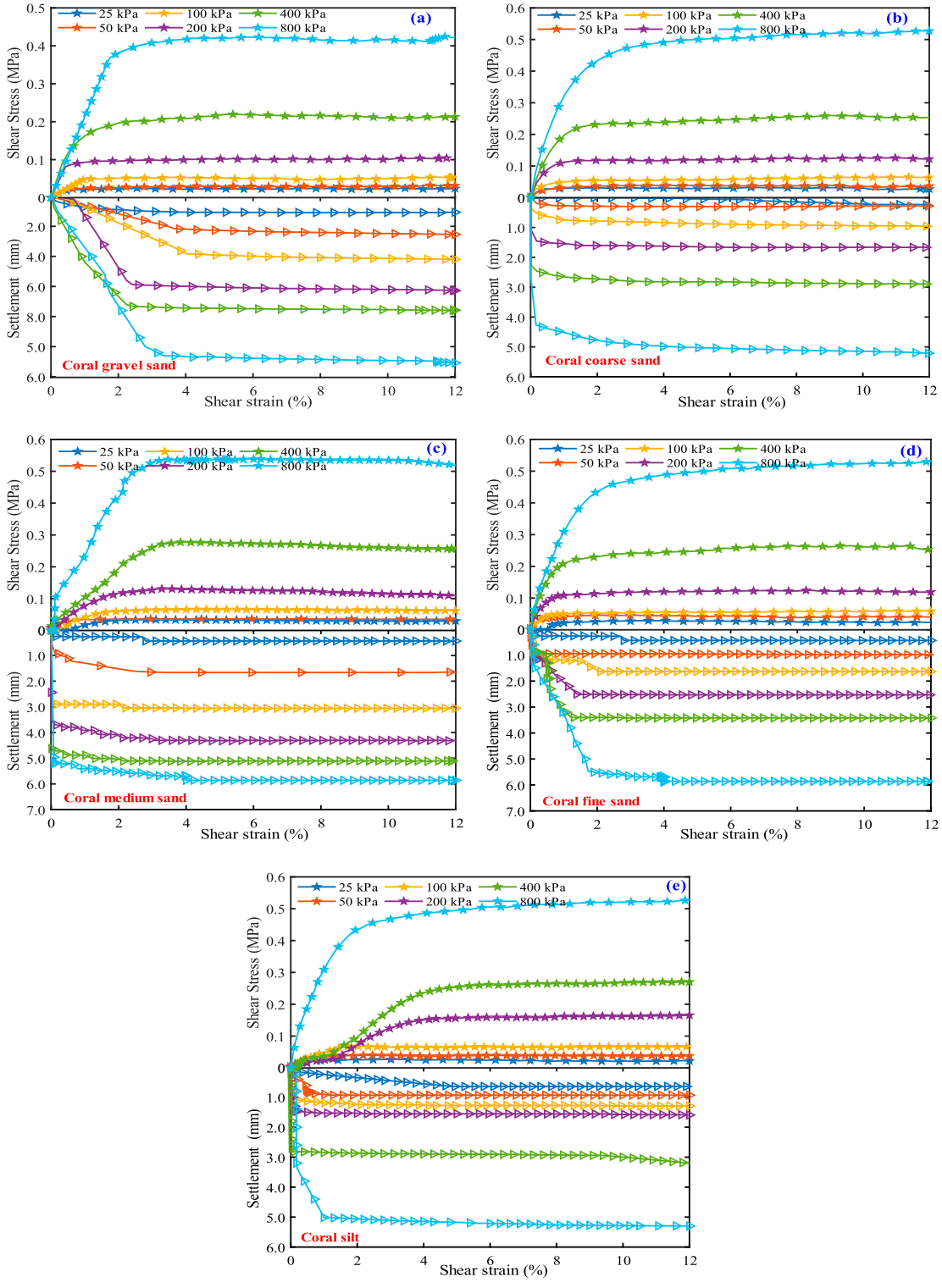

FIGURE 4
Shear deformation at coral sand-concrete interface.

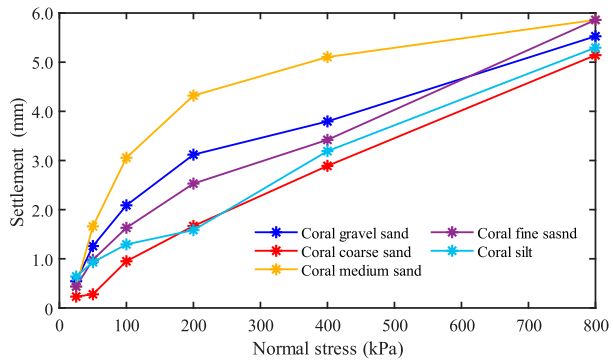

FIGURE 5
Settlement law of coral sand under different stress conditions.

peak strength of the specimen is recommended to be the steady-state strength. This strength regularity of 5 types of coral sand-concrete interfacial shear tests is basically in accordance with the ideal elastic-plastic model. As can be seen from Figure 4, the peak interfacial shear strength of coral sand increases continuously with the growth of strata vertical stress around the pile, and furthermore, the shear strain at the peak strength also increases gradually, and the strain at the turning point of strength curve of all coral sand samples is basically less than 4%.Among the 5 types of coral sands, which include coral gravel sand, coral coarse sand, coral medium sand, coral fine sand, and coral silty, the coral medium sand has the greatest interfacial shear strength under the same test conditions.

As indicated in Figure 4, all 5 types of coral sands undergo distinct settlement behaviors during the shear process, ultimately reaching a stable state. The coral sand particles exhibit a notable fragility, whereby they readily undergo crushing during the shearing process. Subsequently, the crushed particles are redistributed, with the finer particles effectively filling the pores between the original coral sands, leading to both settlement and compaction of the sample. This process underscores the distinct shear-induced contraction characteristic inherent to coral sand. This phenomenon is also common in the research of other scholars (Coop et al., 2004; Gao and Ye, 2023; Li et al., 2023; Wang et al., 2021a).

Figure 5 shows the settlement law of 5 graded coral sands under different stress conditions, and the final settlement is less than 6 mm. Among them, the settlement of coral medium sand is the most obvious, and the settlement of coral coarse sand is the least. It can be seen that the settlement of coral sand is affected by the gradation, but the law is not obvious. Due to the diversity of morphology, high Surface roughness and abundant pores in coral sand particles, the complexity of this material has brought many challenges to practical engineering construction.

Figure 6 demonstrates the relation curves between the interfacial shear strength of 5 types of coral sands and the normal stress. Observations show that the interfacial shear strength of coral sand exhibits a good linear relationship with the normal stress, and the interfacial friction angle ranges from 28° to 35°. As the proportion of fine particles in the coral sand increased, the slope of the peak shear strength of the sample showed an increasing trend, but the increment was small. Due to the presence of more large particles with well-developed internal pores in the coral gravel sand, its strength was lower than that of the other 4 types of coral sand. From the results of Figure 6, the grading of the coral sand has little effect on the interfacial shear behavior between coral sand and concrete, with the applied normal stress being the primary influencing factor of interfacial shear strength.

3.2 Results from crushed coral reef limestone interfacial shear test

Figure 7 demonstrates that the interfacial shear curve of crushed coral reef limestone is similar to that of coral sand. The shear stress-shear strain relationship observed in the crushed coral reef limestone-concrete interfacial shear test also exhibits a nearly ideal elastic-plastic behavior, with the shear strain at the peak stress increasing as the normal stress increases. The settlement variation of crushed coral reef limestone differs significantly from that of coral sand. At the start of the test, crushed limestone produces substantial settlement and maintains a relatively stable state. This may be attributed to the damage and pronounced angularity of the crushed particles. These characteristics lead to a substantial settlement immediately after the initial application of normal stress. Following this initial settlement, the particles interlock with each other, thereby maintaining a relatively stable state. From the settlement law of crushed CRL under different stress conditions shown in Figure 8, it can be seen that as the crushing stress increases, the settlement tends to decrease, and the increase of fine particle content has a moderating effect on the settlement.

The shear strength of the interface between crushed coral reef limestone and concrete is observed to increase linearly with an increase in normal stress. As shown in Figure 9, the shear strength of crushed coral reef limestone exhibits minimal variation under varying crushing stresses, suggesting that the crushing stress exerts limited influence on the interfacial shear behavior between the limestone and concrete. A comparison of the interfacial shear strength results between coral sand and crushed coral reef limestone reveals that the two materials exhibit similar shear characteristics. However, the peak shear strength of coral sand occurs slightly later than that of crushed coral reef limestone, and the difference in the interfacial friction angle between the two is insignificant.

4 SFR of driven pile in coral sand

Crushed coral reef limestone exhibits similar interfacial shear characteristics to coral sand, therefore, the SFR for driven pile

in coral reef limestone can adopt the calculation method that is applicable applicable to coral sand. Due to the complex mechanical characteristics of coral reef strata, a model test has been undertaken to obtain the SFR capacity of prefabricated pipe pile in coral sand strata, Based on this test, the distribution law of pile SFR in coral reef strata is captured, and concurrently, the fitness between coral reef strata and prefabricated pipe pile is analyzed.

4.1 Design of prefabricated pile model test

The samples used in the model test were extracted from uncemented coral medium sand located in the sea area adjacent to the Maldives islands and reefs. These samples exhibit an inhomogeneity coefficient of Cu = 4.88 and a curvature coefficient of Cc = 0.91, which is a poorly graded sand. Three group model pile tests have been devised to investigate the relationship between the SFR of driven piles and the vertical effective stress surrounding the pile. The primary focus of this model test should be on two key aspects: the boundary effects inherent in model testing and the application of vertical effective stress loading around the pile. For the boundary conditions of the model test, with reference to the model size of the similar tests conducted globally (as presented in Table 4), it is recommended that the ratio of the distance B, which separates the model from the box wall, to the model size b should be greater than 3.0. The model box used in this study is a cylinder with a diameter of 2 m and a height of 3 m. Furthermore, the model pile is designed as a prefabricated pipe pile, boasting a maximum outer diameter of 0.25 m and a length of 2.0 m, with B/b=5.5>3, which satisfies the relevant requirements.

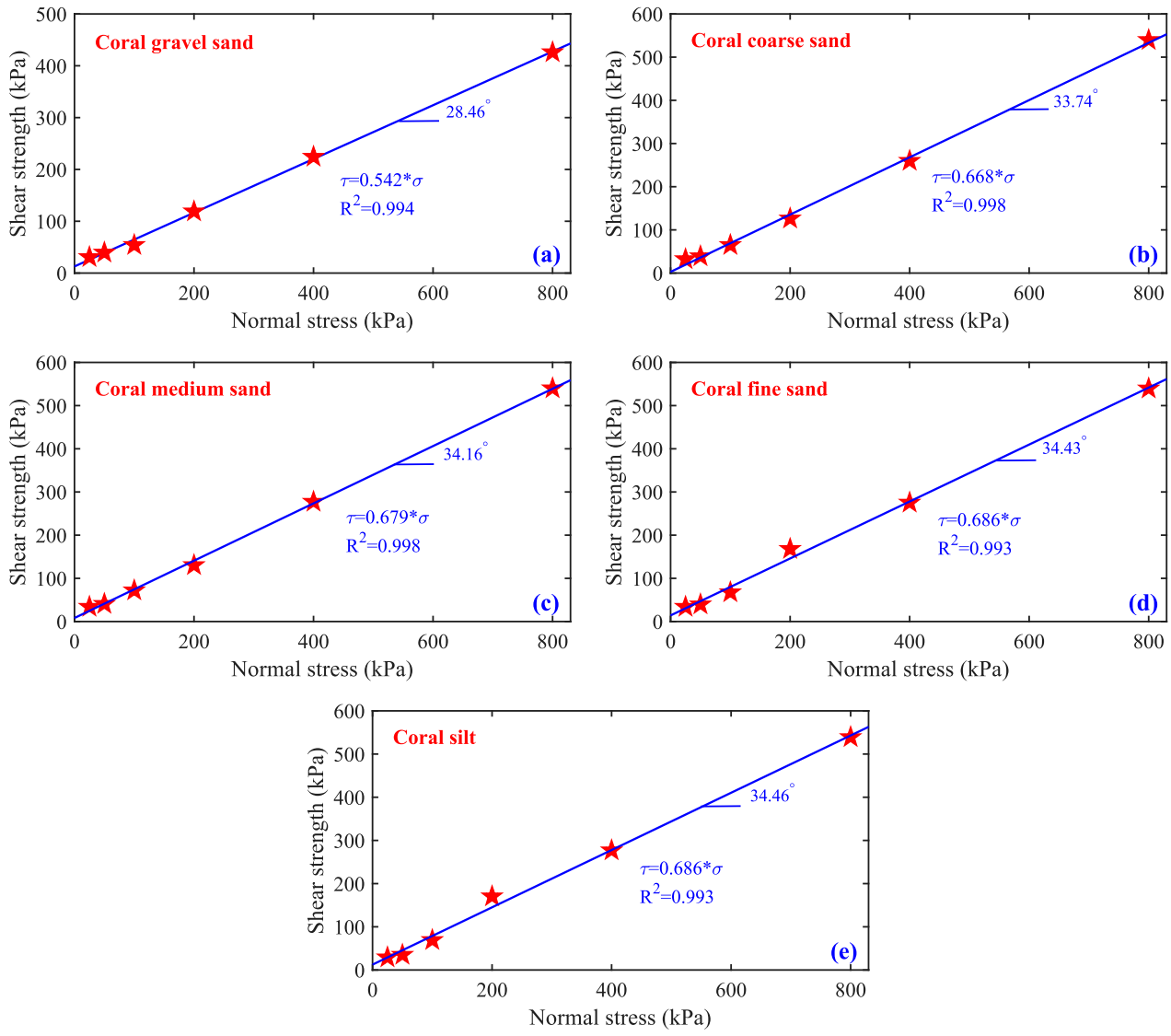

FIGURE 6
Relation curve between the interface shear strength of coral sand and the normal stress.

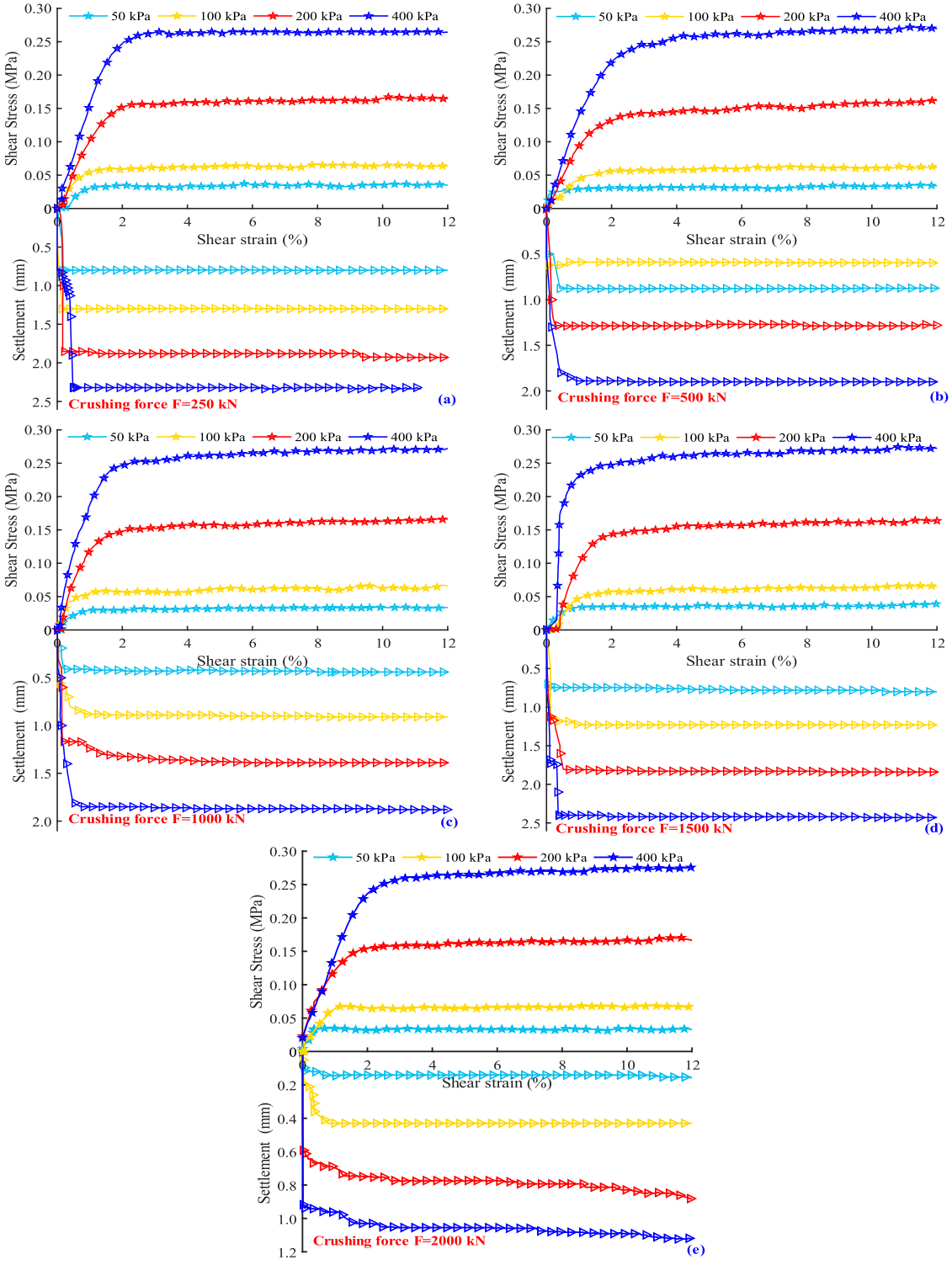

FIGURE 7
Shear deformation at CRL-concrete interface.

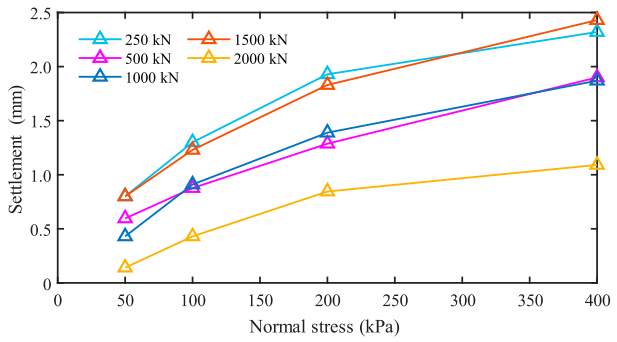

FIGURE 8
Settlement law of crushed CRL under different stress conditions.

To investigate the varying trend of the SFR of pile in coral sand, three groups of model piles with a uniform wall thickness of 40 mm and outer diameters of 250 mm, 192 mm, and 160 mm respectively, are selected and numbered ① to ③ in sequence. Based on the density of coral sand raw material, the dry density of the coral sand layer is set to 1.45 g/cm^3, which is laid with a layer thickness of 250 mm and subsequently compacted. After laying two layers of sand, each with a thickness of 250 mm, totaling 500 mm, the prefabricated model piles are placed vertically into the center of the model box. Following this, the layered filling is continued, and the verticality of the piles is constantly checked until the filling reaches the design elevation, as shown in Figure 10.

The strata stress loading system comprises of the loading plate, the force transfer column, and the strata stress loading jack, as illustrated in Figure 11. The loading plate is a concrete slab featuring a hole at its center, with an outer diameter of 1,900 mm and a thickness of 200 mm, respectively. The force transfer column employs two 2.2-meter-long spliced I-beams, which are connected to the pre-embedded lifting ring of the loading plate via anchoring bolts. Threaded jacks and pressure rings are utilized for loading control, featuring a capacity of 50 t, a stroke of 450 mm and a control accuracy of 0.1 t. The actuator serves the purpose of pile loading, boasting a capacity of 25 t and a control accuracy of 0.1 t. Reinforcement beams and fine-rolled rebars are employed to limit the piles to control the perpendicularity.

The test establishes 8 loading levels of 24 kPa, 36.5 kPa, 49 kPa, 74 kPa, 99 kPa, 124 kPa, 174 kPa, and 224 kPa, to investigate the ultimate SFR and its distribution pattern under varying vertical effective stresses surrounding the pile. The loading rate adopted is 10 kN/min, and the load is maintained for 20 min after each level of loading is completed. The settlement is recorded once the displacement meter reading stabilizes, subsequently proceeding to the application of the next loading level.

The main parameters collected include horizontal and vertical stresses, pile side soil pressure and pile SFR, which are measured by soil pressure cells and a ultra-weak fiber Bragg grating (UWFBG) analyzer, respectively. The arrangement of soil pressure cells is illustrated in Figure 12, and the three layers are positioned at distances of 0.5 m, 1 m, and 1.5 m from the bottom of the box, respectively. The numbers start from the lowest layer and are numbered clockwise from the middle vertical soil pressure cell. The horizontal and vertical soil pressure cells within the same group are positioned at the same elevation to enhance the testing accuracy. The horizontal soil pressure cell is equipped with a protective sleeve to mitigate interference from the vertical pressure. The soil pressure cell is embedded in fine sand to guarantee that the soil pressure is transmitted uniformly to the surface of the cell. The measuring wires are safeguarded by plastic tubes and routed along the inner wall of the model box.

Ultra-weak Fiber Bragg Grating (UWFBG) is an application-specific distributed fiber optic sensor that has been refined based on the sensing principle of Fiber Bragg Grating (FBG). It is capable of accurately measuring variations in strain, temperature, vibration, and other parameters at specific points along the optical fiber, enabling wide-range distributed monitoring (Rao, 1999). This type of sensor is widely employed for monitoring and testing various engineering fields, including civil engineering, composite materials, oil, power, and numerous other sectors (Li et al., 2004; Metje et al., 2006). Additionally, some exploratory applications have been conducted in concrete piles (Kister et al., 2007). The arrangement of UWFBG measurement points is illustrated in Figure 12, where a slot is cut into the exterior of the pile and subsequently filled with AB adhesive. This ensures the coordinated deformation between the grating and the pile. An aluminium alloy shell is installed at the slotting location to prevent extrusion of AB adhesive by the surrounding ground, which could potentially disrupt the coordinated deformation between the grating and the pile. Prior to the test, the test pile is axially loaded using a jack and pressure ring. Additionally, the grating optical fiber is calibrated by comparing the theoretical stress value with the test value obtained from a resistance strain gauge, ensuring the accuracy of the test data.

4.2 Results and analysis

Taking the additional load increment of 99 kPa as an illustrative example, the variation in the test frequency of the soil pressure cell located at model boundary during the entire loading process is presented in Figure13. Upon observation, it is evident that there is no discernible change in the lateral pressure recorded at the model boundary. This finding suggests a minimal boundary effect, thereby validating the rationality of the chosen model dimensions and ensuring the reliability of the test results belonging to the model pile.

The relationship curve between SFR and relative displacements of test piles is presented in Figure 14. The variations in SFR for test piles of three sizes exhibit a similar pattern, where SFR gradually increase and eventually remains stable as the relative pile-soil displacements increase. The increase of strata vertical

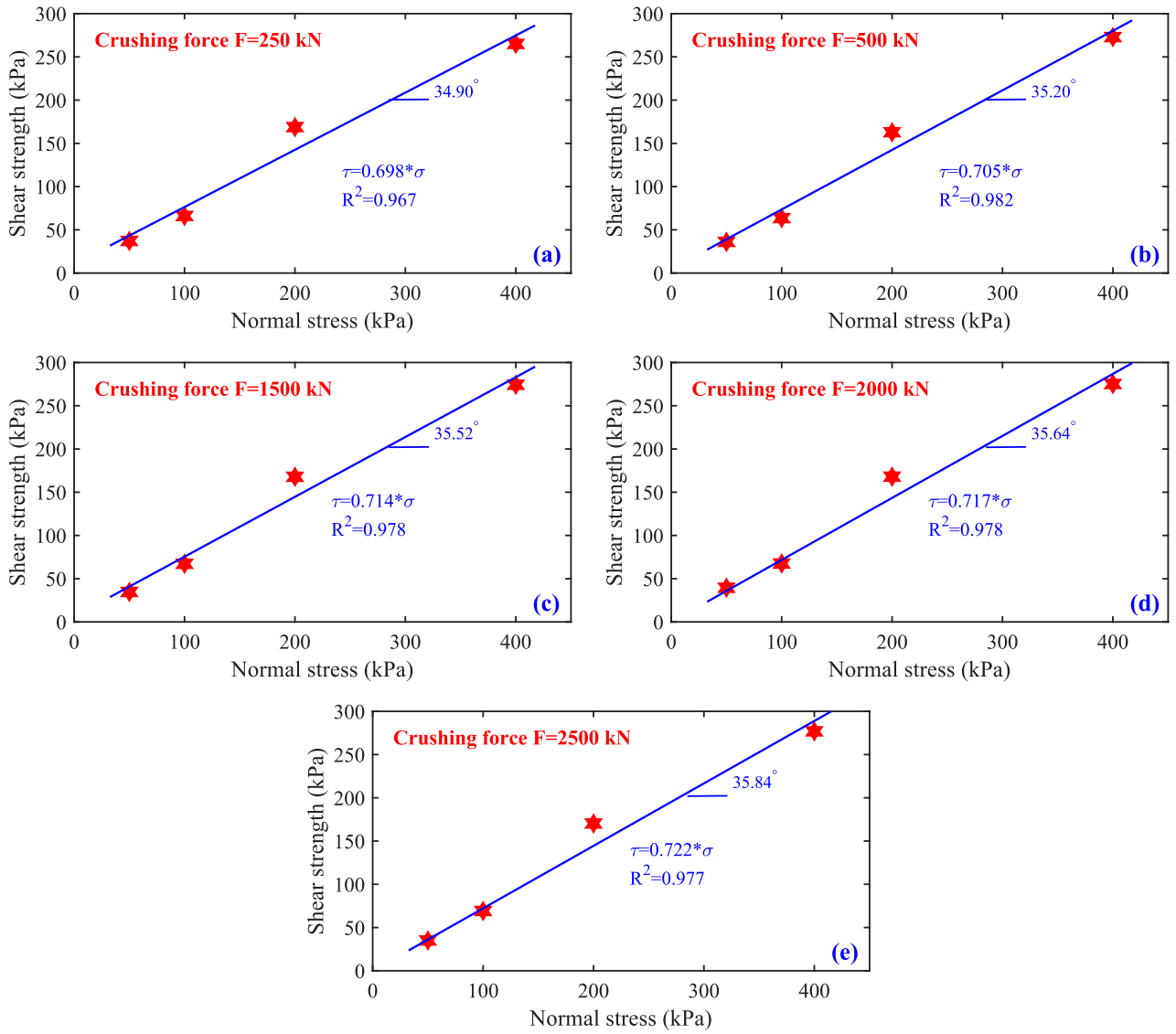

FIGURE 9
Relation curve between the interface shear strength of crushed CRL and the normal stress.

stress around the pile causes the ultimate SFR to increase, and at the same time, the displacement required for the ultimate SFR to be fully realized also begins to decrease. Moreover, with the pile diameter increases, the ultimate SFR and the displacement required to fully realize the ultimate SFR of the pile all increase. In general, increasing the stress of the strata around the pile is beneficial to increase the SFR and reduce the displacement required for the ultimate SFR. Increasing the pile diameter can improve SFR, but the displacement will also increase. The relationship curve between vertical effective stress and ultimate SFR is presented in Figure 15. As vertical stress increases, the ultimate SFR first increases and then tends to stabilize, with a ultimate SFR of about 17.9 kPa.

The variation of pile SFR with vertical effective stress around the pile in quartz medium sand formation is determined according to the recommended method of American Petroleum Institute specification (API, 2000). This is then compared with the results obtained in a coral medium sand formation, as illustrated in Figure 15. In both strata, the pile SFR exhibits a parabolic distribution, and once the ultimate SFR is reached, the pile SFR

10.3389/feart.2024.1481614

TABLE 4 Summary of similar test parameters worldwide.

Size of model box (m)	Pile size (Outside diameter m × Length m)	B/b	Slenderness ratio	Fill around pile
Square:1.2 × 1.8 (Zhao, 2020)	0.032 × 1.05	27.63	32.81	Clay
Circular:$\varphi \times h$=0.7 × 0.9 (Jiang et al., 2018)	0.03 × 0.6	11.17	20	Calcareous sand
Length × Width × Height 2.5 × 2.5 × 3 (Peng, 2018)	0.05 × 0.6	24.50	12	coral sand
	0.05 × 0.9		18	
	0.05 × 1.2		24	
Length × Width × Height 0.8 × 0.8 × 1 (Liu, 2018)	0.04 × 0.7	9.50	17.5	Calcareous sand
Length × Width × Height 0.7 × 0.7 × 1.2 (Li, 2020)	0.03 × 0.3	11.17	10	Calcareous sand
	0.03 × 0.6		20	
	0.03 × 0.9		30	
	0.02 × 0.4	17.00	20	
Length × Width × Height 0.9 × 0.9 × 1 (Qin et al., 2015)	0.032 × 0.5	13.56	15.6	Calcareous sand
	0.032 × 0.7		21.8	
Length × Width × Height 2 × 2 × 3 (Chen et al., 2018)	0.06 × 1.004	16.17	16.7	Calcareous sand
Length × Width × Height 0.8 × 0.8 × 1 (Liu JY et al., 2021)	0.05 × 0.40	7.5	8	Calcareous sand
	0.05 × 0.55		11	
	0.05 × 0.70		14	

FIGURE 10
Model pile installation and layered vibration.

ceases to increase further with increasing depth. Compared with quartz medium sand, the SFR of prefabricated pile in coral sand is lower, accounting for approximately 21.4% of that in quartz medium sand. This value is close to the 27% result obtained in a test conducted by Jiang et al. (2018). Through stress conversion, the depths at which the ultimate SFR is reached in coral medium sand and quartz medium sand are approximately 9.3 m and 25 m, respectively.

The critical depth for achieving the pile ultimate SFR in coral medium sand is lower than that in quartz medium sand, and the incremental rate of the SFR for piles in coral reef medium sand is about 16% of that in the quartz medium sand. This phenomenon is primarily attributed to the fact that the large internal friction angle and occlusion force of coral sand cause the particles to be susceptible to the formation of a circular arch effect during deformation, resulting in little or no increase in the lateral pressure increment.

4.3 Calculation method of SFR of prefabricated pile in coral reef strata

At present, there is no effective calculation method for the SFR of pile foundations in coral reef strata in China,

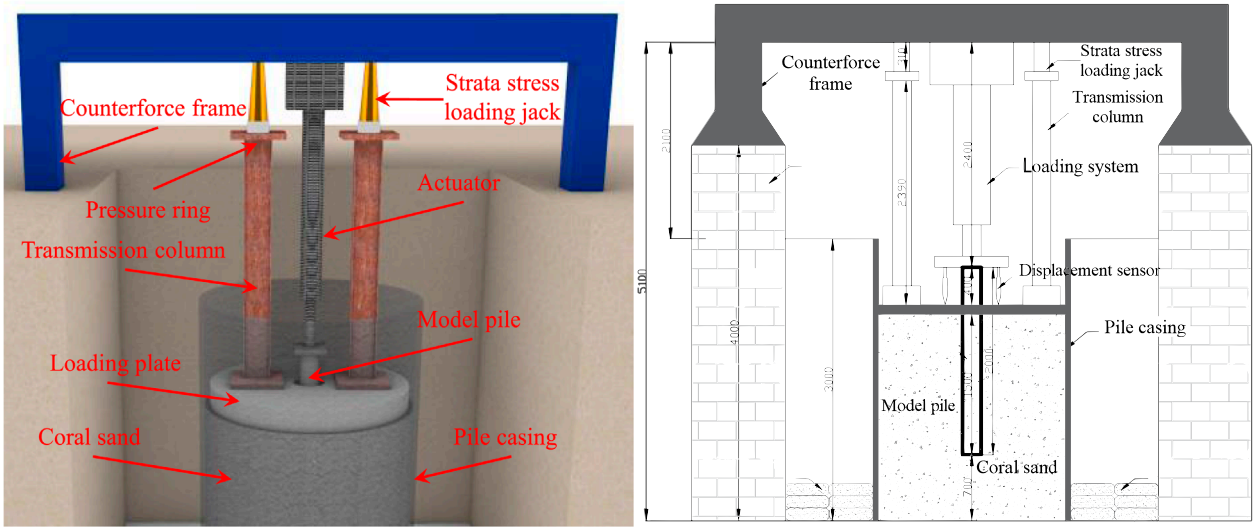

FIGURE 11
Test device and device diagram.

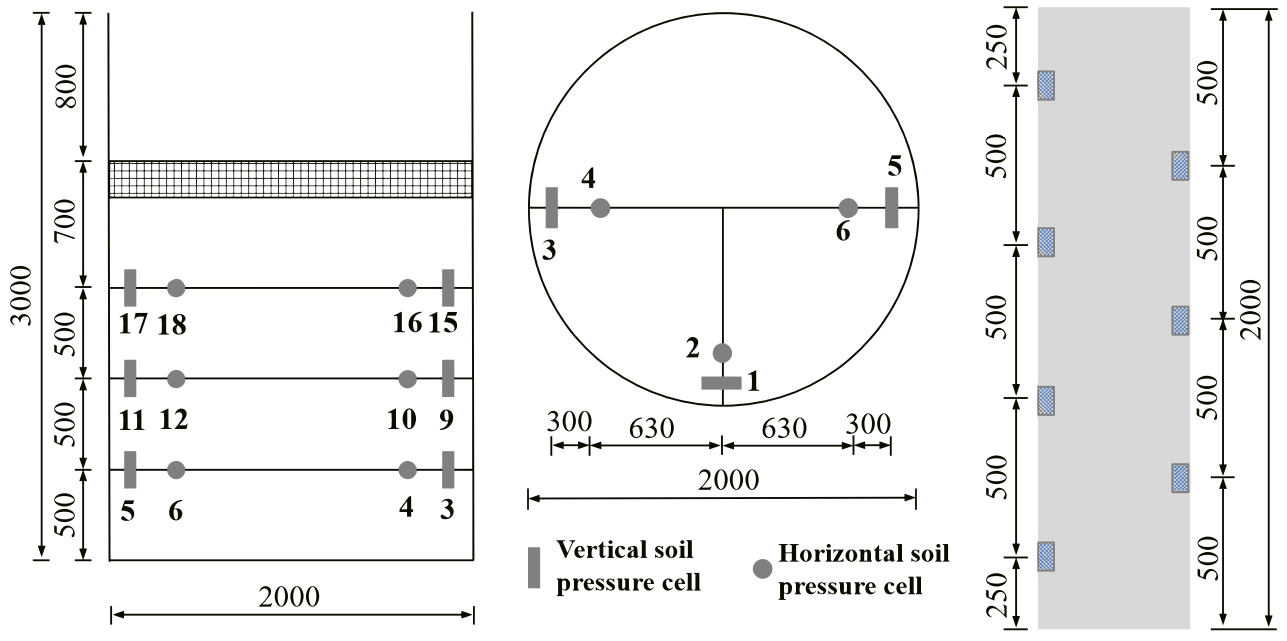

FIGURE 12
Arrangement of soil pressure cell and fiber grating measuring point (unit: mm).

while the recommended method in API specification that primarily adjusts the parameters of the lateral pressure coefficient k, the friction angle δ between the soil and the pile wall, the ultimate unit SFR fmax, and the ultimate unit end resistance qmax is commonly adopted in the international community.

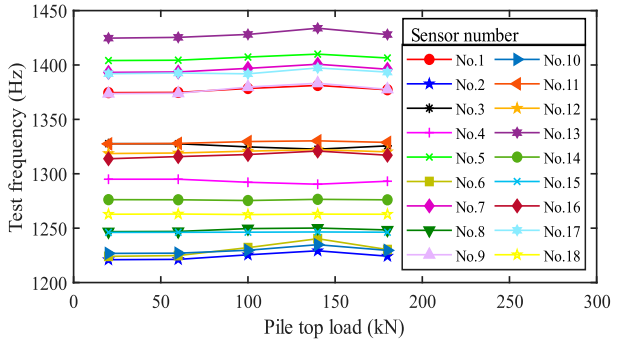

FIGURE 13
Frequency variation of soil pressure cell.

Based on the test results, the distribution of SFR is simplified to a combination of triangle and rectangle mode, and a calculation method is proposed, with reference to the API specification, as illustrated in Equations 1–3.

$$q_s = \begin{cases} \sigma_n' \tan\delta = K_0 \sigma_v' \tan\delta & (h < H_0) \\ \eta \dfrac{Y}{1+\alpha} \tan\delta & (h \geq H_0) \end{cases} \quad (1)$$

$$\alpha = \frac{1+\sin\varphi}{1-\sin\varphi} \quad (2)$$

$$Y = \frac{2C\cos\varphi}{1-\sin\varphi} \quad (3)$$

Where σ_n' is the vertical effective self-gravitational stress of the soil on the pile side; δ is the interfacial friction angle; K_0 is the static lateral pressure coefficient of the soil; σ_v' is the horizontal stress of the soil on the pile side; η is the comprehensive modification coefficient for pile-soil contact and pile foundation squeezing strata; C and φ are cohesion and internal friction angle, respectively.

As the depth increases, the circular arch effect of coral sand is more pronounced, resulting in a corresponding increase in the ultimate SFR of the pile. Considering the complexity of the calculation process of the circumferential compressive stress coefficient, the depth at which the theoretical value of shallow SFR is equal to the theoretical value of deep SFR is taken as the critical depth to simplify the calculation, which can be calculated by Equation 4.

$$H_0 = \frac{\eta Y}{(1+\alpha)\gamma K_0} \quad (4)$$

The data obtained from this model test have been utilized to validate the applicability of the proposed method for calculating pile SFR. The calculation results are presented in Table 5 and Figure 16. Specifically, when the contact comprehensive correction coefficient is η = 2, the ultimate pile SFR is 16.54 kPa, whereas the average measured ultimate pile SFR is 17.4 kPa, with an error of 5.2%. The growth rates of calculated and measured SFR values with respect to depth are 0.13 and 0.16, respectively, yielding an error of 18.8%. The calculated critical depth is 16.7 m, which is greater than the measured value of 9.3 m, indicating that the calculation method is reasonable and the calculation result is on the safe side.

Thirty-two protecting tubes of the China-Maldives Friendship Bridge are selected as the research subjects, and the SFR calculation method for driven piles in coral reef strata, proposed in this study, is employed to calculate the SFR capacity of driven piles of China-Maldives Friendship Bridge. Comparison of the calculation results with the monitored results from the field test pile is shown in Figure 17. The deviation between the theoretical value and the measured value is within 20%, and the average deviation is 10.3%, the theoretical values are consistently smaller than the measured ones. This indicates that the calculation method proposed in this study is conservative and reasonable. Considering that the complexity of the coral reef sand strata on site is much higher than that of the test strata, and the actual construction of the pile length is large, this calculation method is acceptable for safety considerations.

5 Discussion

In this investigation, a series of experiments were conducted to examine the SFR capacity of prefabricated pipe piles in coral reef strata. The findings indicate that the variability in SFR for pile foundations within coral reef geological conditions exhibits a pattern similar to that observed in terrestrial strata. Consistent with prior research, the diameter of the pile and the stress distribution around the pile emerge as predominant factors influencing the SFR (Ding et al., 2021; Liu et al., 2023). However, compared to terrestrial sand, the SFR of prefabricated pipe piles in coral reef geological conditions is significantly lower than that predicted by existing specifications. This discrepancy can be primarily attributed to the highly irregular morphology and rough surface texture of coral sand particles, which result in substantial intergranular interlocking and occlusion. Consequently, coral sand exhibits pronounced structuration characteristics. These properties facilitate the formation of a circular arch effect, thereby leading to negligible increments in lateral pressure (Altuhafi et al., 2018; Wang et al., 2022). The limitations of this research are delineated as follows: The geological complexity of coral reef formations at actual engineering sites presents substantial challenges. Coral reef limestone exhibits considerable heterogeneity in strength, characterized by a wide distribution of internal pores. At present, the SFR of prefabricated pipe piles embedded within coral reef limestone cannot be accurately quantified. Future investigations should focus on rock-socketed piles in coral reef limestone to optimize the calculation methods for the SFR of prefabricated pipe pile. Such studies should take into account the integrity and pore distribution characteristics of reef limestone to better understand and model the behavior of these structures.

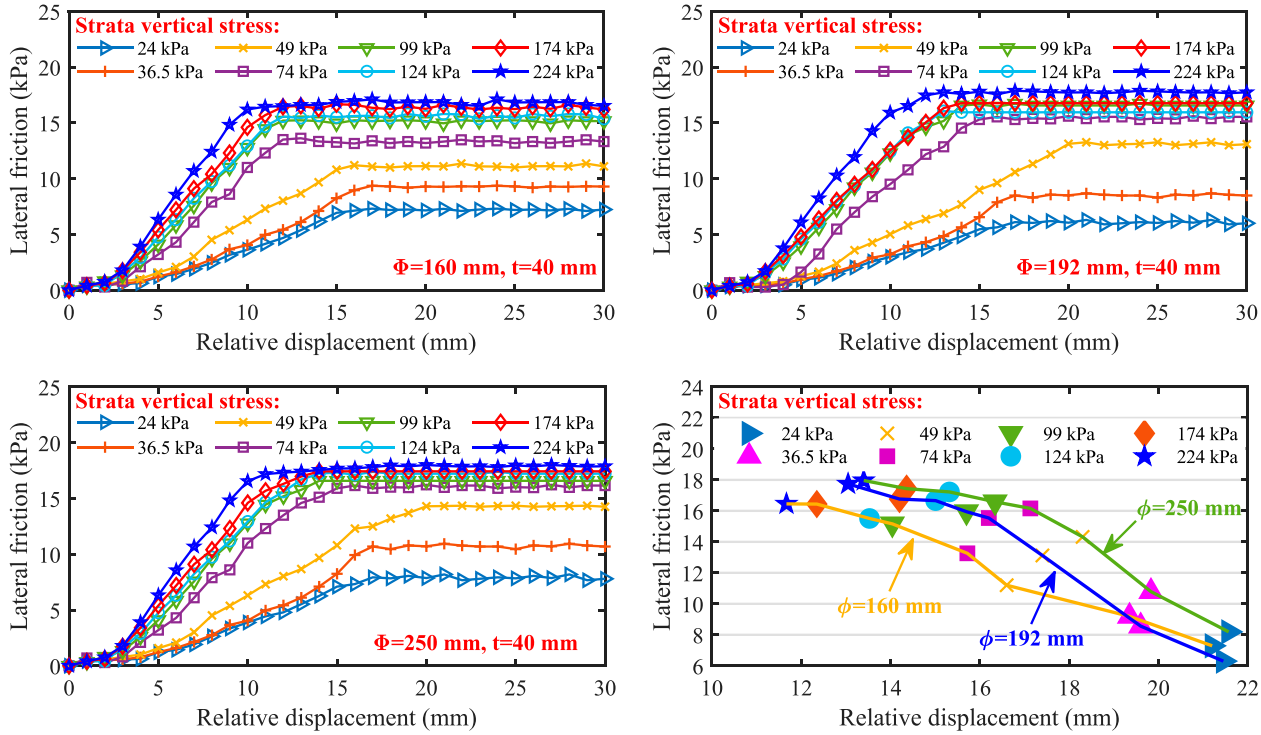

FIGURE 14
Test curves of SFR and relative pile-soil displacement.

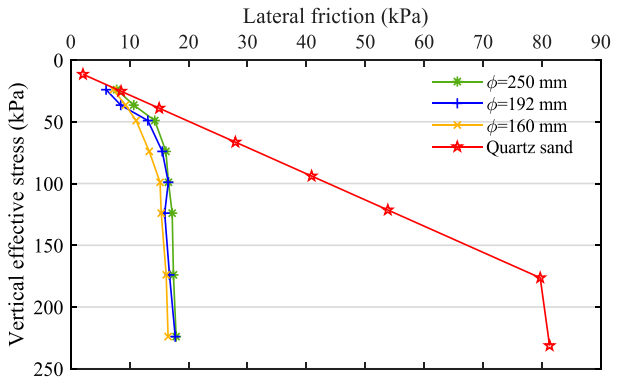

FIGURE 15
Relationship between vertical effective stress and ultimate SFR.

6 Conclusion

In this study, a series of interfacial shear tests were conducted on coral sand and coral reef limestone extracted from the sea area near the Maldives islands and reefs. Additionally, the distribution of SFR of prefabricated pipe piles embedded in coral sand was investigated utilizing a large-scale pile foundation model test apparatus. The following conclusions are obtained:

(1) The interfacial shear patterns of coral sand and crushed coral reef limestone are similar, both exhibiting ideal elastic-plastic characteristics, characterized by an interfacial friction angle of approximately 35°.

(2) The SFR of prefabricated piles in coral sand initially increases and eventually stabilizes as the relative pile-soil displacement increases. The distribution of SFR along the depth direction can be simplified as a combination of triangular and rectangular mode. The ultimate SFR gradually increases and then tends to stabilize with increasing depth. The final ultimate SFR is approximately 17.9 kPa, which is only 20%–30% of that observed in similar land-sourced sands.

(3) A modified formula for calculating the SFR of the piles in coral sand has been established based on the test results of pile foundation. The SFR capacity of the driven piles of the China-

TABLE 5 Calculated SFR values of the pile in coral sand.

Soil	Internal friction angle φ (°)	Cohesion C (kPa)	Interfacial friction angle δ (°)	Static lateral pressure coefficient K_0	Critical vertical effective stress (kPa)	Shallow ultimate SFR	Deep SFR (kPa)
Coral medium sand	45.3	22.4	27.7	0.25	98	$0.131\sigma_v$	8.27η

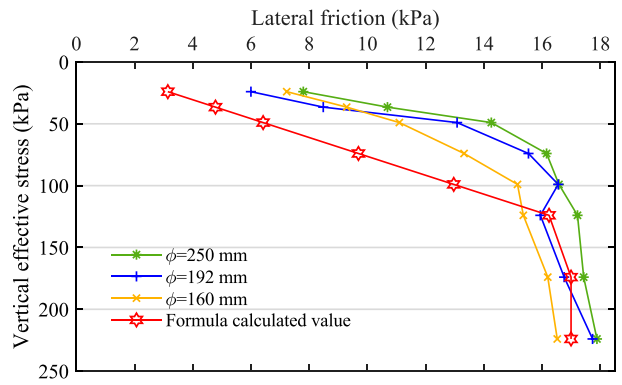

FIGURE 16
Comparison between the calculated and experimental values of ultimate pile SFR.

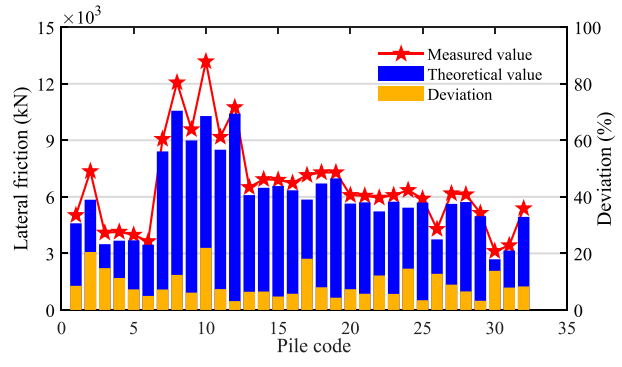

FIGURE 17
Comparison of calculated and measured pile SFR.

Malaysia Friendship Bridge is calculated and compared with the results of field test piles, which verified the reasonableness of the proposed calculation method.

Data availability statement

The original contributions presented in the study are included in the article/supplementary material, further inquiries can be directed to the corresponding author.

Author contributions

HZ: Conceptualization, Methodology, Project administration, Supervision, Writing–review and editing. RG: Data curation, Formal Analysis, Investigation, Methodology, Validation, Visualization, Writing–original draft, Writing-review and editing. HuL: Methodology, Writing–review and editing. PC: Project administration, Writing–review and editing. HaL: Methodology, Writing–review and editing.

Funding

The author(s) declare that no financial support was received for the research, authorship, and/or publication of this article.

Conflict of interest

Authors HZ, RG, HuL, and PC were employed by CCCC Second Harbour Engineering Company Ltd.

The remaining author declares that the research was conducted in the absence of any commercial or financial relationships that could be construed as a potential conflict of interest.

Publisher's note

References

Achmus, M., Kuo, Y.-S., and Abdel-Rahman, K. (2009). Behavior of monopile foundations under cyclic lateral load. *Comput. Geotechnics*, 725–735. doi:10.1016/j.compgeo.2008.12.003

Agarwal, S.-L., Malhotra, A.-K., and Banerjee, R.-L. (1977). Engineering properties of calcareous soils affecting the design of deep penetration piles for offshore structures. *Offshore Technol. Conf.* doi:10.4043/2792-MS

Altuhafi, F.-N., Jardine, R.-J., Georgiannou, V.-N., and Moinet, W.-W. (2018). Effects of particle breakage and stress reversal on the behaviour of sand around displacement piles. *Géotechnique* 68 (6), 546–555. doi:10.1680/jgeot.17.P.117

Angemeer, J., Carlson, E.-D., Stroud, S., and Kurzeme, M. (1975). Pile load tests in calcareous soils conducted in 400 feet of water from a semi-submersible exploration rig. *Offshore Technol. Conf.* doi:10.4043/2311-MS

API (2000). "Recommended practice for planning, designing and constructing fixed offshore platforms-working stress design," in *Api RP2A*. Washington, D.C.: American Petroleum Institute.

Bi, J., Zhou, X.-P., and Qian, Q.-H. (2015). The 3D numerical simulation for the propagation process of multiple pre-existing flaws in rock-like materials subjected to biaxial compressive loads. *Rock Mech. Rock Eng.* 49 (5), 1611–1627. doi:10.1007/s00603-015-0867-y

Chen, Y., Yang, M., Wei, H.-Z., Li, W.-C., and Meng, Q.-S. (2018). Experimental study on axial tension response of model monopile in calcareous sand. *Rock Soil Mech.* 39, 2851–2857. doi:10.16285/j.rsm.2018.0569

Chortis, G., Askarinejad, A., Prendergast, L.-J., Li, Q., and Gavin, K. (2020). Influence of scour depth and type on p-y curves for monopiles in sand under monotonic lateral loading in a geotechnical centrifuge. *Ocean. Eng.* 197, 106838. doi:10.1016/j.oceaneng.2019.106838

Coop, M.-R., Sorensen, K.-K., Bodas Freitas, T., and Georgoutsos, G. (2004). Particle breakage during shearing of a carbonate sand. *Geotechnique* 54 (3), 157–163. doi:10.1680/geot.2004.54.3.157

Ding, X.-M., Deng, W.-T., Peng, Y., Zhou, H., and Wang, C.-Y. (2021). Bearing behavior of cast-in-place expansive concrete pile in coral sand under vertical loading. *China Ocean. Eng.* 35 (3), 352–360. doi:10.1007/s13344-021-0038-8

Ding, X.-M., Deng, X., Ou, Q., and Deng, W.-T. (2023). Experimental study on the behavior of single pile foundation under vertical cyclic load in coral sand. *Ocean. Eng.* 280, 114672. doi:10.1016/j.oceaneng.2023.114672

Dutt, R.-N., and Cheng, A.-P. (1984). Frictional response of piles in calcareous deposits. *Offshore Technol. Conf.* doi:10.4043/4838-MS

Dyson, G.-J., and Randolph, M.-F. (2001). Monotonic lateral loading of piles in calcareous sand. *J. Geotechnical Geoenvironmental Eng.* 127, 346–352. doi:10.1061/(ASCE)1090-0241(2001)127:4(346)

Fahey, M., and Jewell, R.-J. (1988). "Model pile tests in calcarenite," in *Proceedings of international conference on calcareous sediments*. Perth, 555–564.

Fan, S.-Y., Song, Z.-P., Wang, H.-Z., Zhang, Y.-W., and Zhang, Q. (2023). Influence of the combined action of water and axial pressure on the microscopic damage and mechanical properties of limestone. *Geoenergy Sci. Eng.* 228, 212027. doi:10.1016/j.geoen.2023.212027

Gao, R., and Ye, J.-H. (2023). Mechanical behaviors of coral sand and relationship between particle breakage and plastic work. *Eng. Geol.* 316, 107063. doi:10.1016/j.enggeo.2023.107063

Ghazali, F.-M., Sotiropoulos, E., and Mansour, O.-A. (1988). Large-diameter bored and grouted piles in marine sediments of the Red Sea. *Can. Geotechnical J.* 25, 826–831. doi:10.1139/t88-090

Guo, W.-D. (2006). On limiting force profile, slip depth and response of lateral piles. *Comput. Geotechnics* 33, 47–67. doi:10.1016/j.compgeo.2006.02.001

Guo, Z.-Y., Khidri, M., and Deng, L.-J. (2018). Field loading tests of screw micropiles under axial cyclic and monotonic loads. *Acta Geotech.* 14, 1843–1856. doi:10.1007/s11440-018-0750-6

Ho, H.-M., Malik, A.-A., Kuwano, J., Brasile, S., Tran, T.-V., and Mazhar, M.-A. (2022). Experimental and numerical study on pressure distribution under screw and straight pile in dense sand. *Int. J. Geomechanics* 22 (9), 04022139. doi:10.1061/(ASCE)GM.1943-5622.0002520

Höppner, R., and Boley, C. (2022). Erkenntnisse zum tragverhalten von fertigschraubpfählen unter axialer belastung. *Bautechnik* 99 (9), 656–664. doi:10.1002/bate.202200030

Jiang, H., Wang, R., Lv, Y.-H., and Meng, Q.-S. (2018). Test study of model pile in calcareous sands. *Rock Soil Mech.* 31, 780–784. doi:10.16285/j.rsm.2010.03.040

Karthigeyan, S., Ramakrishna, V. V. G. S. T., and Rajagopal, K. (2006). Influence of vertical load on the lateral response of piles in sand. *Comput. Geotechnics* 33, 121–131. doi:10.1016/j.compgeo.2005.12.002

Kister, G., Winter, D., Gebremichael, Y.-M., Leighton, J., Badcock, R.-A., Tester, P.-D., et al. (2007). Methodology and integrity monitoring of foundation concrete piles using Bragg grating optical fibre sensors. *Eng. Struct.* 29, 2048–2055. doi:10.1016/j.engstruct.2006.10.021

Kong, D., and Fonseca, J. (2018). Quantification of the morphology of shelly carbonate sands using 3D images. *Géotechnique* 68 (3), 249–261. doi:10.1680/jgeot.16.P.278

Li, H.-N., Li, D.-S., and Song, G.-B. (2004). Recent applications of fiber optic sensors to health monitoring in civil engineering. *Eng. Struct.* 26, 1647–1657. doi:10.1016/j.engstruct.2004.05.018

Li, W., and Deng, L. (2018). Axial load tests and numerical modeling of single-helix piles in cohesive and cohesionless soils. *Acta Geotech.* 14 (2), 461–475. doi:10.1007/s11440-018-0669-y

Li, W.-J. (2020). *Research on model test of bearing characteristics of post grouting pile in calcareous sand formation*. Guilin: Guilin University of Technology.

Li, X.-B., Zhang, R.-Y., Yang, Z., Chen, P.-S., Ji, F.-Q., and Wen, B. (2023). Mechanical behavior analysis and bearing capacity calculation of CFG pile composite foundation on coral sand site. *Front. Earth Sci.* 11, 1204989. doi:10.3389/feart.2023.1204989

Lin, X.-F., Zhang, J.-S., Wang, R.-S., Zhang, J., Liu, W., and Zhang, Y.-Q. (2019). Scour around a mono-pile foundation of a horizontal axis tidal stream turbine under steady current. *Ocean. Eng.* 192, 106571. doi:10.1016/j.oceaneng.2019.106571

Liu, H.-F., Zhu, C.-Q., Wang, R., Cui, X., and Wang, T.-M. (2021). Characterization of the interface between concrete pile and coral reef calcarenite using constant normal stiffness direct shear test. *Bull. Eng. Geol. Environ.* 80, 1757–1765. doi:10.1007/s10064-020-02039-8

Liu, J.-Y. (2018). *Research on vertical bearing properties of x-section pile foundation in calcareous sand*. Chongqing: Chongqing University.

Liu, J.-Y., Wang, C.-Y., Liu, M.-Y., Ding, X.-M., and Liu, H. (2021). Horizontal loading model test of single pile in calcareous sand. *J. Civ. Environ. Eng.* 43, 74–81. doi:10.11835/j.issn.2096-6717.2021.049

Liu, S.-M., Sun, H.-T., Zhang, D.-M., Yang, K., Li, X.-L., Wang, D.-K., et al. (2023). Experimental study of effect of liquid nitrogen cold soaking on coal pore structure and fractal characteristics. *Energy* 275, 127470. doi:10.1016/j.energy.2023.127470

Malik, A.-A., Kuwano, J., Tachibana, S., and Maejima, T. (2016). End bearing capacity comparison of screw pile with straight pipe pile under similar ground conditions. *Acta Geotech.* 12, 415–428. doi:10.1007/s11440-016-0482-4

Metje, N., Chapman, D.-N., Rogers, C.-D.-F., Henderson, P., and Beth, M. (2006). Optical fibre sensors for remote monitoring of tunnel displacements-Prototype tests in the laboratory. *Tunn. Undergr. Space Technol.* 21, 417. doi:10.1016/j.tust.2005.12.062

Peng, Y., Yin, Z.-Y., and Ding, X.-M. (2023). Micromechanical analysis of the particle corner breakage effect on pile load performance in coral sand. *Acta Geotech.* 18, 6353–6370. doi:10.1007/s11440-023-01975-5

Peng, Y.-X. (2018). *Experimental research on penetration mechanism of driving steel pipe pile in coral calcareous sands*. Nanjing: Southeast University.

Poulos, H.-G., and Randolph, M.-F. (1988). Evaluation of pile friction from conductor tests. *Int. Conf. Calcareous Sediments*, 599–605.

Qin, W., Dai, G.-L., Ma, L.-Z., Pei, M.-H., Wang, L., and Zhu, G.-Y. (2019). *In-situ* static loading tests of prestressed high strength concrete (PHC) pile in coral strata. *Rock Soil Mech.* 40, 381–389. doi:10.16285/j.rsm.2019.0149

Qin, Y., Meng, Q.-S., Wang, R., and Zhu, C.-Q. (2015). A study on bearing characteristics of single pile in calcareous sand based on model experiment. *Rock Soil Mech.* 36, 1714. doi:10.16285/j.rsm.2015.06.025

Rao, Y.-J. (1999). Recent progress in applications of in-fibre Bragg grating sensors. *Opt. Lasers Eng.* 31, 297–324. doi:10.1016/S0143-8166(99)00025-1

Schmüdderich, C., Shahrabi, M.-M., Taiebat, M., and Lavasan, A.-A. (2020). Strategies for numerical simulation of cast-in-place piles under axial loading. *Comput. Geotechnics* 125, 103656. doi:10.1016/j.compgeo.2020.103656

Song, Z.-P., Zhang, A., Li, G.-X., Liu, S.-J., and Zhang, J.-B. (2018). Study of seawater corrosion resistance of ordinary Portland cement-aluminate cement-gypsum mortar containing slag. *Adv. Cem. Res.* 32 (4), 196–204. doi:10.1680/jadcr.18.00008

Wang, C.-Y., Ding, X.-M., Cao, G.-W., Jiang, C.-Y., Fang, H.-Q., and Wang, C.-L. (2022). Numerical investigation of the effect of particle gradation on the lateral response of pile in coral sand. *Comput. Geotechnics* 152, 105012. doi:10.1016/j.compgeo.2022.105012

Wang, C.-Y., Ding, X.-M., Xiao, Y., Peng, Y., and Liu, H.-L. (2021a). Effects of relative densities on particle breaking behaviour of non-uniform grading coral sand. *Powder Technol.* 382, 524–531. doi:10.1016/j.powtec.2021.01.015

Wang, C.-Y., Liu, H.-L., Ding, X.-M., Wang, C.-L., and Ou, Q. (2021b). Study on horizontal bearing characteristics of pile foundations in coral sand. *Can. Geotechnical J.* 58, 1928–1942. doi:10.1139/cgj-2020-0623

Wang, X., Wang, X.-Z., Zhu, C.-Q., and Meng, Q.-S. (2019). Shear tests of interfaces between calcareous sand and steel. *Mar. Georesources & Geotechnol.* 37, 1095–1104. doi:10.1080/1064119X.2018.1529845

Xu, M., Zhang, F., Ni, P., and Mei, G. (2023). Load-settlement behaviour of membrane-confined grouted pile: experimental and analytical study. *Acta Geotech.* 18 (5), 2777–2793. doi:10.1007/s11440-022-01711-5

Xu, X.-L., Lei, X., Wang, T.-L., Kong, G.-Q., and Li, C.-H. (2022). Experimental study on shear mechanical properties of pile-coral sand interface. *Chin. J. Undergr. Space Eng.* 18, 1891–1897+1905.

Yao, T., Cao, Z.-W., and Li, W. (2024). On the mechanical behaviour of a coral silt from the South China Sea. *Géotechnique*, 1–14. doi:10.1680/jgeot.24.00012

Zhao, C.-N. (2020). Model test study on bearing capacity of single pile under cyclic loading in loess foundation. *Masteral Diss*.

Zhao, Y., Bi, J., Wang, C., and Liu, P. (2021). Effect of unloading rate on the mechanical behavior and fracture characteristics of sandstones under complex triaxial stress conditions. *Rock Mech. Rock Eng.* 54 (9), 4851–4866. doi:10.1007/s00603-021-02515-x

Zhou, B., Ku, Q., Li, C., Wang, H., Dong, Y., and Cheng, Z. (2022). Single-particle crushing behaviour of carbonate sands studied by X-ray microtomography and a combined finite-discrete element method. *Acta Geotech.* 17 (8), 3195–3209. doi:10.1007/s11440-022-01469-w

Zhou, Y. (2014). *Theoretical analysis and experimental studies on residual stress of jacked open-ended concrete pipe piles*. Hangzhou: Zhejiang University.

Zhu, C.-Q., Zhou, B., and Liu, H.-F. (2015). State-of-the-art review of developments of laboratory tests on cemented calcareous soils. *Rock Soil Mech.* 36, 311–319+324. doi:10.16285/j.rsm.2015.02.002